Extension of the operating space of high-β_N fully non-inductive scenarios on TCV using neutral beam injection

C. Piron[1,2], J. Garcia[3], M. Agostini[1], M. Fontana[4], G. Giruzzi[3], M. Gobbin[1], T. P. Goodman[4], A. N. Karpushov[4], M. Kong[4], A. Merle[4], J. Morales[3], S. Nowak[5], L. Pigatto[1], O. Sauter[4], D. Testa[4], M. Vallar[1], M. Yoshida[6], the TCV team and the EUROfusion MST1 team[7]

[1]Consorzio RFX (CNR, ENEA, INFN, Università di Padova, Acciaierie Venete SpA) Corso Stati Uniti 4 - 35127 Padova, Italy, [2] ENEA, Fusion and Nuclear Safety Department, C. R. Frascati, Via E. Fermi 45, 00044 Frascati (Roma), Italy, [3]CEA, IRFM, F-13108 Saint Paul Lez Durance, France, [4]Ecole Polytechnique Fédérale de Lausanne (EPFL), Swiss Plasma Center (SPC), CH-1015 Lausanne, Switzerland, [5]Istituto di Fisica del Plasma IFP-CNR, I-20125 Milano, Italy, [6]National Institutes for Quantum and Radiological Science and Technology, Naka, Ibaraki 311-0193, Japan, [7]See the author list "H. Meyer et al 2017 Nucl. Fusion 57 102014"

E-mail: chiara.piron@igi.cnr.it

May 2019

Abstract. The fully non-inductive sustainment of high normalized beta plasmas (β_N) is a crucial challenge for the steady-state operation of a tokamak reactor. In order to assess the difficulties facing such scenarios, steady-state regimes have been explored on the Tokamak à Configuration Variable (TCV) using the newly available 1 MW Neutral Beam Injection (NBI) system. The operating space is extended towards plasmas that are closer to those expected in JT-60SA and ITER, i.e. with significant NBI and Electron Cyclotron Resonance Heating and Current Drive (ECRH/CD), bootstrap current and Fast Ion (FI) fraction. β_N values up to 1.4 and 1.7 are obtained in lower single null L-mode ($H_{98}(y,2) \sim 0.8$) and H-mode ($H_{98}(y,2) \sim 1$) plasmas, respectively, at zero time averaged loop voltage and $q_{95} \sim 6$. Fully non-inductive operation is not achieved with NBI alone, whose injection can even increase the loop voltage in the presence of EC waves. A strong contribution to the total plasma pressure of thermal and FIs from NBI is experimentally evidenced and confirmed by interpretative ASTRA and NUBEAM modeling, which further predicts that FI charge-exchange reactions are the main loss channel for NBH/CD efficiency. Internal transport barriers, which are expected to maximize the bootstrap current fraction, are not formed in either the electron or the ion channel in the plasmas explored to date, despite a significant increase in the toroidal rotation and FI fraction with NBI, which are known to reduce turbulence. First results on scenario development of high-β_N fully non-inductive H-mode plasmas are also presented.

1. Introduction

The fully non-inductive sustainment of high normalized beta (β_N) plasmas is a crucial challenge for the steady-state operation of a tokamak reactor. In this scenario the plasma current is sustained without any external poloidal magnetic flux consumption for several characteristic plasma current diffusion times. To achieve a time-averaged zero toroidal loop voltage (V_{loop}), the maximization of poloidal beta (β_θ) is also appropriate in order to maximize the fraction of bootstrap current and alleviate the necessity of external current drive. However, such a process is notoriously complicated due to the exacting physics requirements: high input power and plasma confinement, current alignment between bootstrap current and current drive and MHD control. In order to assess the difficulties faced by such scenarios and to extend previous steady-state plasmas obtained with only Electron Cyclotron Resonance Heating (ECRH), steady-state regimes have been explored at the Tokamak à Configuration Variable (TCV) using the newly available Neutral Beam Injection (NBI) system [1]. This system supplies up to 1 MW (25 keV) to the plasma by accelerating positive deuterium ions. Due to machine protection constraints [2, 3], the maximum NB injected energy was initially limited to 0.5 MJ and relaxed to 0.8 MJ after NBI optimizations for experiments presented in this work. Since the beam duct port is installed on the torus middle plane, off-axis NBI is obtained on TCV by vertically shifting the plasma magnetic axis (z). Values up to |z| = 13 cm have been explored for a plasma half-height of around 0.4 m. In this work, fully non-inductive operation is achieved with additional 3.2 MW of ECRH power [4], which is transferred to the plasma through both X2 (P = 2.3 MW) and X3 (P = 0.9 MW) waves. Unless otherwise specified, the power values that appear in this work correspond to the injected power. The X3 waves do not provide any net current drive in the plasmas presented here, as their wave vector aims at the plasma core perpendicularly to the magnetic field to maximize the power absorption. Notably even with oblique injection X3 wave absorption on TCV is not generally strong enough to occur fully on one side of the resonance and thereby selectively heat the electrons moving in one direction. The X2 and X3 cut-off is $n_e > 4.3 \times 10^{19} m^{-3}$ and $n_e > 1.1 \times 10^{20}\ m^{-3}$, respectively. This paper presents the first results that have been achieved during the dedicated experiments of the 2017/18 EUROfusion MST1 campaign on TCV and is organized as follows: Section 2 describes the explored plasma scenarios and presents the resulting extended operating space. The role of the NBI to both plasma pressure and current drive is investigated and documented with data analysis and modeling in Section 3. The challenge of generating Internal and External Transport Barriers (I/ETBs), which are crucial for improving the plasma confinement and the total fraction of non-inductive current drive, is discussed in Section 4. The summary and outlook are eventually given in Section 5.

2. The extended operating space

Compared to the past, when fully non-inductive plasmas were sustained using EC waves only on TCV [5, 6], the operating space has been now extended towards higher density ($n_{e,0} = 2 - 3 \times 10^{19}\ m^{-3}$) at currents of $130 - 150$ kA using co-Ip NBI; this produces plasmas closer to those expected in JT-60SA and in ITER, i.e. with significant NBI and ECRH current drive, bootstrap current and fast ion fraction. This new plasma scenario is designed to minimize the first-orbit and shine-through beam losses. Furthermore, Lower Single Null (LSN) plasmas at $B_{\Phi,0} = 1.4$ T [7] were chosen over the more extensively studied limiter ones, since a lower neutral penetration from the edge is expected to reduce the Charge eXchange (CX) beam losses [8]. Both L-mode and H-mode plasmas at $q_{95} = 5-6$ have been explored. The latter will be presented in Section 4. A representative Ip = 130 kA L-mode discharge is shown in Fig.1. As it can be inferred from the time evolution of the loop voltage (panel c)), stationary fully non-inductive operation is achieved in this experiment for around 10 current diffusion times ($\tau_\eta \simeq 150$ ms on TCV plasmas with auxiliary heating) by combining 2.3 MW of on-axis ECRH power (1.4 MW from X2 waves and 0.9 MW from X3 waves) with 0.8 MW of off-axis NBI power ($z \simeq 9$ cm), both injected in the co-Ip direction. The time evolution of the injected powers together with the LSN equilibrium reconstructed by LIUQE [9] at t = 1.25 s are reported in panel b). The plasma current is over-driven in this discharge by the auxiliary systems during $t = (1.05, 1.65)$ s, as it can be seen from the decrease of the edge poloidal magnetic flux (panel c)), which is due to the on-going recharge of the Ohmic transformer. During this time window, the bootstrap current fraction is around 30% (panel a)), $H_{98}(y, 2) = 0.85$ and $\beta_N = 1.35$ (panel d)).

The performance of the plasmas explored in this work is summarized in Fig.2, which plots β_N versus V_{loop}, both averaged over 15 ms around each acquisition time of the Thomson Scattering diagnostic. The exploration of the operating space has been carried out by carefully scanning $P_{aux} = P_{EC} + P_{NB}$, the NB power fraction (P_{NB}/P_{aux}) and the radial deposition locations of the NB and EC Heating and Current Drive (H/CD). β_N values up to 1.4 have been achieved in stationary fully non-inductive L-mode plasmas at $H_{98}(y, 2) \sim 0.8$. Higher total pressure $\beta_N = 1.7$ and confinement $H_{98}(y, 2) \sim 1$ have been obtained in nearly non-inductive conditions ($V_{loop} \sim 80$ mV) in the in the TCV H-mode plasmas at Ip=150 kA. In both cases the best performance is obtained with central EC and NBI H/CD in the co-Ip direction, which results to $f_{BS} \simeq 30\%$. For comparison, it is worth noticing that $\beta_N < 0.4$ and $V_{loop} > 0.7$ V are typically obtained in similar Ohmic plasmas (blue points, color online). As it will be discussed further on, the NB injection in presence of EC waves can both increase or decrease, though weakly, V_{loop} depending on its radial deposition. The effect of the NB power fraction on V_{loop} is almost negligible in presence of ECRH, while it clearly increases the thermal and fast ion pressure, and thereby β_N, in the plasmas explored in this work.

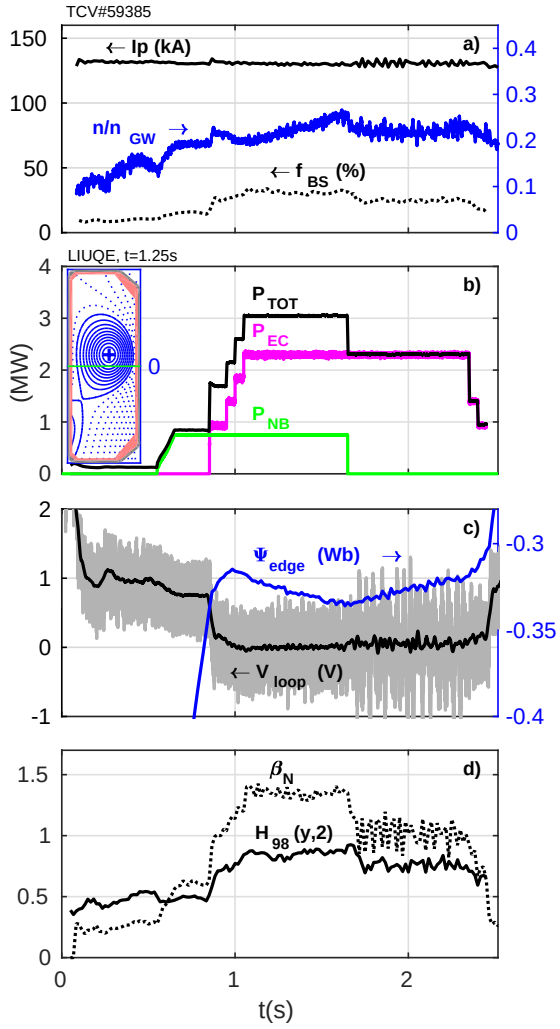

Figure 1: Time evolution of a) plasma current and bootstrap current fraction (solid and dotted black lines on the left y-axis) and the Greenwald density fraction (blue on the right y-axis); b) ECRH (magenta), NB (green) and total (black) power, LIUQE equilibrium at t = 1.25 s with a poloidal view of the NB injection line (solid green line) in the inserted plot on the left; c) the raw and the time-averaged loop voltage (in gray and black on the left y-axis) and the edge poloidal flux (in blue on the right y-axis); d) $H_{98}(y, 2)$ and β_N (solid and dotted black line).

3. The role of the Neutral Beam Injection in the scenario development

3.1. NBI contribution to the total plasma pressure

Statistical analysis of experimental data shows that the highest β_N does not necessarily correspond to the maximum electron thermal energy. This suggests a strong contribution of thermal and Fast Ions (FIs) to the total plasma pressure. This experimental evidence is reproduced by ASTRA [12] and NUBEAM [13, 14] interpretative modeling.

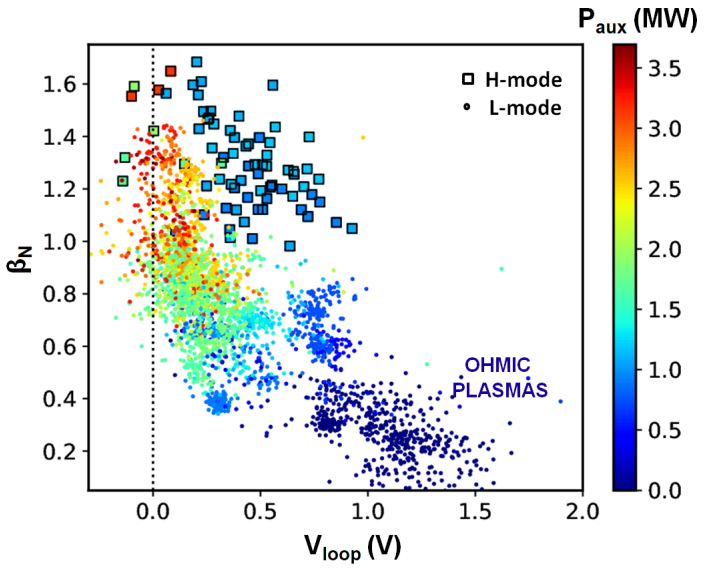

Figure 2: β_N versus loop voltage in the explored L-mode (small circles) and H-mode (big squares) plasmas. The color code corresponds to the auxiliary power.

Simulations, like the one shown in Fig.3 a), predict a large population of FIs with a core density ($\rho < 0.15$) comparable to the thermal ions (panel a)). Notably, the total ion density is lower than the electron one during NBI as the effective ion charge Z_{eff} increases from ~ 1.4 to ~ 2 at $t > 0.7$ s. The energy and density of the cold incoming neutrals have been estimated in this simulation using the 1D kinetic transport code KN1D [10] and the measurement by baratron pressure gauges [11]. Despite the fairly good agreement between the simulated and the diagnostic data, more accurate FI models taking into account the FI-to-FI collisions are required in ASTRA and NUBEAM to properly simulate this regime on TCV. Modeling further reveals that FI charge-exchange is the main loss channel reducing NB heating efficiency, as can be seen in panel b) which shows the time evolution of the different NB power redistribution channels. 80 kW, 12 ms blips of the 50 keV hydrogen diagnostic neutral beam modulate the NB power from t $>$ 0.5 s. A large FI contribution and significant CX losses were also observed in inductive L-mode plasmas in a circular limited configuration at TCV [15]. Nonetheless, a quantitative comparison of the NBI performance on limiter and lower single null plasma equilibria is not straightforward due to the significantly different plasma parameters that were explored in the corresponding scenarios.

3.2. NBI contribution to the non-inductive current drive

Developing a steady-state scenario at high β_N is a complex task. Indeed adding NBI results in an increase or decrease of V_{loop} depending on other plasma parameters, such as the plasma vertical position, the electron temperature (T_e) and density and the presence of ECR-H/CD. Fully non-inductive operation could not be achieved with NBI

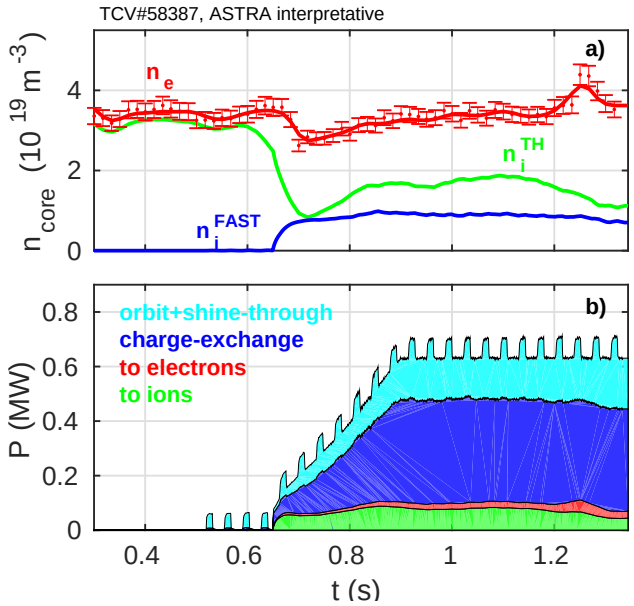

Figure 3: Interpretative ASTRA simulation of a NBI heated TCV L-mode discharge. Time evolution of a) electron (red, data with errorbars from the Thomson Scattering diagnostic), thermal ion (green) and fast ion (blue) core density; b) NBI power redistribution channels: power to ions (green) and electrons (red), charge-exchange (blue), first ion orbit and shine-through (cyan) losses.

alone ($V_{loop} > 0.5$ V). Data analysis of the explored plasmas shows that the V_{loop} drop during the NBI is more rapid at lower density when adding NBI to the Ohmic phase. Nonetheless, it is worth noticing that the density cannot be arbitrarily decreased, being limited by the maximum shine-through power loss limit ($P_{ST} < 10\%$). Fig.4 shows the averaged absolute loop voltage variation (ΔV_{loop}) that is obtained during the injection of ~ 0.7 MW of NB power as a function of a diagnostic proportional estimate of the Spitzer's NB slowing down time [16] in the plasma core, which is quantified here as $T_{e,0}^{3/2} n_{e,0}^{-1}$. Panel a) and b) correspond to plasmas without and with ECRH, respectively. In the former ΔV_{loop} is evaluated compared to the Ohmic phase ($\Delta V_{loop} = V_{loop}^{NBI} - V_{loop}^{OH}$), while in the latter to the ECRH one ($\Delta V_{loop} = V_{loop}^{NBI+ECRH} - V_{loop}^{ECRH}$). In order to properly define a threshold between on-axis and off-axis NB injection in the plasmas investigated in this work, interpretative ASTRA simulations similar to that of Fig.3 have been analyzed to determine at which shift of the vertical magnetic axis (|z|) the resulting NB-H/CD and FI density profiles start peaking outwards. Values of |z| at 0, 5, 7.5, 10, 12.5 and 15 cm have been explored, using the same EC-H/CD, n_e and T_e profiles of the simulation in Fig.4. According to the simulations, the boundary between on/off-axis is for |z| in between 7.5 and 10 cm. The threshold is set to the upper bound average of 9 cm in this work. Off-axis NB injection data (|z| $>$ 9 cm) are marked as empty diamonds, while on-axis ones (|z| $<$ 9 cm) as filled triangles. Fig.4 a) suggests that an optimal balance between the non-inductive current drive and the NB slowing time can be found using NBI both on-axis and off-axis, which decreases ΔV_{loop} by up to ~ 0.32 V.

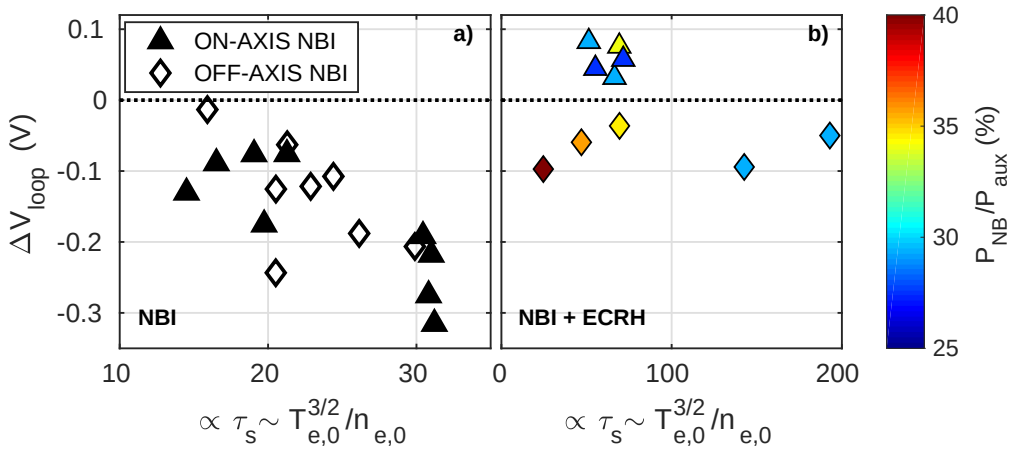

Figure 4: Absolute loop voltage change as a function of a proportional estimate of the NB slowing time on TCV L-mode plasmas. On-axis NBI data are marked as triangles, off-axis ones as diamonds. Panel a) refers to plasmas with NBI only, while panel b) to plasmas with both NBI and ECRH. The color code in panel b) corresponds to the NB power fraction.

Conversely, no clear dependence of the loop voltage variation on the NB slowing down time is observed in the presence of EC waves, as shown in panel b). Interestingly, the loop voltage increases with on-axis NBI while it decreases with off-axis injection, yet only up to -0.1 V. As the color code suggests, no effect can be measured on V_{loop} with a relative change of the NB power fraction $\lesssim 13\%$ (light blue and brown diamonds).

These results have been investigated with ASTRA interpretative modeling of equilibrium, thermal ion temperature and FIs. The results for a representative discharge are reported in Fig.5. In the first part of this experiment, nearly fully non-inductive operation is achieved by launching around 1.6 MW of EC power from X2 waves at $\rho \simeq 0.35$ (in panels a, d)). As a result the loop voltage drops from around $\simeq 0.9$ V to nearly zero (panel b)). During the second phase (t=(0.8, 1.2) s), 0.45 MW of EC power from X3 waves is launched aiming at the plasma core. In this phase, the loop voltage is not affected, since these waves do not provide any net current drive to the plasma on TCV. Interestingly, V_{loop} clearly increases during the last part of the experiment, when the same amount of NB power is deposited on-axis to replace P_{EC-X3}. A possible explanation for the observed V_{loop} increase is provided in the following. The core density is generally pumped out during ECRH on TCV [17], this occur also in this experiment as it can be seen from the hollow electron temperature profile at t = 0.88 s (panel e)). This mechanism naturally helps achieve high electron temperature plasmas (panel c)) and thereby high core ECCD efficiency ($j_{ECCD} \sim T_e/n_e$, panel d) from the linear TORAY-GA ray tracing code [18]). On the other hand NB injection is a rather effective fueling source in this plasma, indeed the electron density in the core increases up to 30%. As a result, the core plasma density is both pumped out by the EC waves and re-fueled by the NBI when both the auxiliary systems are switched on at t > 1.4 s. The latter effect clearly dominates in this experiment, indeed the density peaks and the j_{ECCD} profile

dramatically decreases in amplitude while moving outwards. Ultimately, V_{loop} increases as a consequence of the reduced ECCD efficiency. The q-profile relaxes from weakly reversed to fully monotonic (panel f)). Within the modeling accuracy, this evidence might explain why internal transport barriers, for which the q-profile reversal is crucial [19], were not observed in the plasmas explored up to date, an excessive on-axis NBCD being detrimental to their onset, as previously shown in modeling [20]. In principle, this counteracting interplay between the ECCD efficiency and the NBI fueling can be regulated by either moving the NB deposition more off-axis or/and increasing the EC power. The first solution has not been very effective in the plasmas explored up to date, since the NB deposition is rather broad and the drivent current is weak, therefore only slightly negative ΔV_{loop} values (diamonds in Fig.4 b)) can be achieved. The second one will be attempted in future experiments, exploting the foreseen upgrade of the ECRH system [21].

4. On the creation of transport barriers

Plasmas with transport barriers are characterized by improved confinement and a large fraction of self-driven bootstrap current, which make such scenarios promising candidates for continuous operation. When Internal or/and External Transport Barriers (I/ETBs) originate in a plasma, turbulent transport is generally reduced in the plasma core or/and at the edge, respectively. An optimized shaping of current density and pressure profiles and a good alignment of the large fraction of bootstrap current with their gradients are crucial for achieving significant improvements in particle and energy confinement, as well as in self-current drive. In this work high-beta fully non-inductive scenarios with either ITB or ETB have been explored using both ECRH and NBI H/CD. The results are presented and discussed in the following sections.

4.1. Internal Transport Barriers (L-mode)

The creation of ITBs turned out to be a challenge as they were not formed in either the electron or the ion channel in the plasmas explored to date; and this in spite of a significant increase in the toroidal rotation and FI fraction with NBI, which are known to reduce turbulence [23]. The increase of the former is documented in Fig.6, which shows the core toroidal plasma rotation measurements from the Charge eXchange Recombination Spectroscopy (CXRS) as a function of the total power $P_{TOT} = P_{OH} + P_{EC} + P_{NB}$. The color code highlights the NB power fraction. Positive (negative) velocity values correspond to a toroidal rotation in the opposite, cnt-Ip, (same, co-Ip) direction of the plasma current ($I_p < 0$). Toroidal rotation velocity values of around 20 km/s in the cnt-Ip direction are obtained during the Ohmic phase of the plasmas explored in this work. The toroidal rotation reverts its direction in the presence of co-Ip ECRH or/and NBI, but the maximum values are obtained with NBI only, which accelerates the plasma core up to 200 km/s in the co-Ip direction with 1 MW on-axis

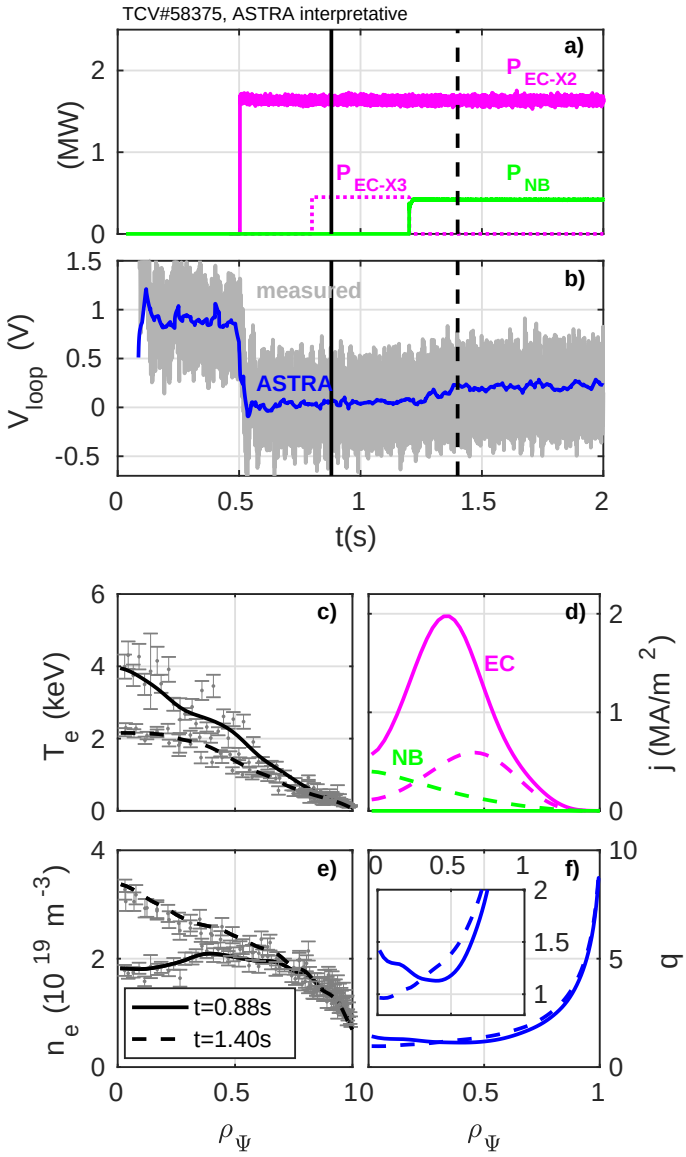

Figure 5: Time evolution of a) ECRH (in magenta, from X2 and X3 waves in solid and dashed line) and NBI (in green) power; b) measured (in gray) and the ASTRA (in blue) loop voltage; c, e) the electron temperature and density profiles from the Thomson Scattering diagnostic; d) NB from ASTRA (in green) and EC from TORAY-GA (in magenta) current density profiles; f) q-profile from ASTRA. Solid lines for t = 0.88 s before NBI, dashed lines for t = 1.40 s during NBI.

injection of NB power.

To investigate the possibility that the plasmas explored in this work are still Trapped Electron Mode (TEM) turbulence dominated, hence less prone to both NB torque and FI stabilization, transport and turbulence analyses were started. Some of the most representative plasmas with different ECRH/CD and NBI configurations were selected for such analysis. From the turbulence point of view, the plasmas shown in this paper are interesting as they combined mostly electron heating with a significant toroidal

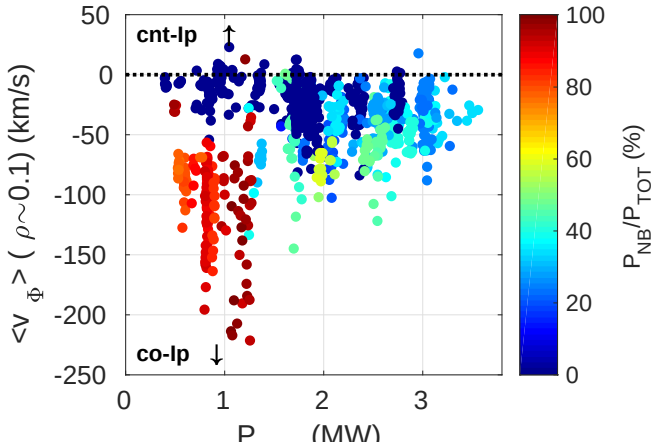

Figure 6: TCV core plasma toroidal rotation from CXRS as a function of the total power $P_{TOT} = P_{OH} + P_{EC} + P_{NB}$. The color code corresponds to the NB power fraction.

rotation and fast ion fraction, which have been shown to reduce turbulence that is driven only by the Ion Temperature Gradient (ITG) modes [23]. Therefore, the analyses of the impact of such turbulence suppression mechanisms can be extended to other plasma regimes. For that purpose, the CRONOS suite of codes [24] is applied here both to perform transport analyses and as a tool for the preparation of the inputs required for extended gyrokinetic simulations. As a first step, CRONOS predictive simulations of current and electron and ion temperatures have been performed. Transport is modeled using the Current Diffusion Ballooning Mode (CDBM) model [27], which is known to capture the transition to ITB regimes well but also gives reasonable results for regular L-mode plasmas. The ECRH/CD source is calculated with REMA [25, 26], a code for ray tracing and relativistic damping of electron cyclotron waves with a linear estimate of the ECCD efficiency. NBI injection is modeled with NUBEAM. Fig.7 shows the first results from a predictive CRONOS simulation of the plasma discharge reported in Fig.5. Panel a) shows that the electron temperature profiles from the Thomson Scattering diagnostic are well reproduced by the CDBM model both in presence of ECRH waves only (at t = 0.88 s) and with NBI (at t = 1.40 s). Nonetheless, the model underestimates the ion temperature profiles in presence of NBI, as it is shown in panel b), which compares the model results with the CXRS data. The origin of such disagreement is due to the approximation made by the CDBM model in calculating the turbulent thermal diffusivity. In fact a single diffusivity is calculated from the model, which is then used in solving both ion and electron energy equations. This approximation limits the applicability of the model, indeed the results of the validation of Fig.7 suggest that it is not adequate for low density plasmas, where T_e and T_i differ significantly. Modeling work is on-going to improve the accuracy of the CRONOS prediction for both species. [R1C4, R2C14].

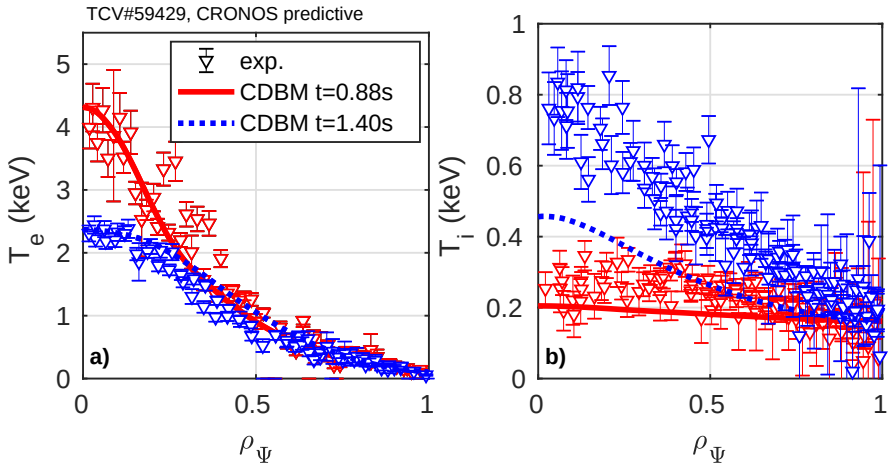

Figure 7: CRONOS predictive simulation of the a) electron and b) ion temperature profiles of the discharge reported in Fig.5 during ECRH (t = 0.88 s, from CDBM model in solid red line) and during ERCH and NBI (t = 1.40 s, from CDBM model in dotted blue line). Experimental data (triangles) from a) the Thomson Scattering and b) the CXRS diagnostic, respectively.

4.2. External Transport Barriers (H-mode)

Thanks to the newly available NBI system, the operating space of high-beta fully non-inductive scenarios could be extended for the first time on TCV towards H-mode plasmas. This scenario aims at β_N values higher than 2.5, i.e. at plasma pressure values closer to those expected in ITER during steady state operation at fusion gain Q $>$ 5 [28]. Due to the elusive character of ITBs, the envisaged H-mode target scenario on TCV are plasmas with ETBs only at low central magnetic shear and $1 < q_0 < 2$. A challenging, yet possible, strategy to reproduce such scenario is to develop plasmas whose density remains lower than the X2 wave cut-off even after the L/H-mode transition, so that ECCD can still contribute to the total non-inductive current drive fraction. One of the first attempts at employing this strategy is shown in Fig.8. In this lower single null discharge at $q_{95} \simeq 5$, relatively high pressure ($\beta_N = 1.7$) and good confinement ($H_{98}(y,2) = 1$) (panel e)) are sustained for several current diffusion times at nearly zero time averaged loop voltage (panel a)) using nearly central co-Ip ECRH and NBI. The former is supplied from both X2-waves (P = 0.9 MW) and X3-waves (P=0.45 MW) while the NB power is around P=1.1 MW (panel b)). The L/H-mode transition occurs a half current diffusion time after the NB injection, during this time the NB absorbed power increases up to 30% according to ASTRA modeling. As it is highlighted in the enlargement reported in panel d) type-I Edge Localized Modes (ELMs) appear during H-mode, whose frequency is increased by the additional heating power from X3-waves, which is switched on slightly afterwards.The electron density at the pedestal (panel d)) almost doubles during H-mode, while the electron and ion temperature (panel c)) increase by nearly 50%. The global effect on the corresponding profiles is plotted in Fig.9. The electron density and temperature are from the Thomson Scattering diagnostic, while

the ion temperature is from the CXRS diagnostic. Core measurements from the latter are not available since the diagnostic NBI is installed at the mid-plane and the plasma vertical axis is slightly vertically shifted (|z| = 3 cm). The measurements are averaged over the L-mode (in blue) and the H-mode (in red) phase. It is worth noticing that the electron density remains below the X2 cut-off even during H-mode (panel a)).

ASTRA interpretative modeling during the H-mode phase of this discharge (t = 1.24 s) is reported in Fig.10, which shows the ECRH, NBI and bootstrap current density profiles during H-mode and the resulting q-profile, which is slightly reversed in the core and close to 1 up to the normalized poloidal radius $\rho_\Psi \simeq 0.5$. Further scenario development is needed to meet the target, i.e. a more highly elevated q-profile with a lower central magnetic shear. The stationarity of this H-mode plasma is limited in this discharge by the MHD activity, indeed a 6 kHz n=1 neoclassical tearing mode, which is likely triggered by the central EC power deposition, eventually locks to the wall ending the plasma discharge.

5. Conclusions

The operating space of high β_N fully non-inductive scenarios has been extended on TCV using the newly available 1 MW NBI system. Plasma regimes closer to those expected in JT-60SA and ITER have been explored, i.e. with significant NBI and ECRH current drive, bootstrap current and fast ion fraction. β_N values up to 1.4 and 1.7 have been reached in fully non-inductive L-mode plasmas and nearly fully H-mode plasmas respectively, both at $q_{95} = 5 - 6$ and in presence of good confinement ($H_{98}(y,2) \simeq 0.8$ during L-mode and $H_{98}(y,2) \simeq 1$ during H-mode) using central EC and NB H/CD in the co-Ip direction, which results in $f_{BS} \lesssim 30\%$. Fully non-inductive operation could not be achieved with NBI alone. The plasma loop voltage increases with on-axis NBI while it decreases, though weakly, by moving outwards the beam injection in presence of EC waves. Data analysis and interpretative ASTRA modeling confirm this evidence, which is due to an interplay between the plasma density pump-out from ECRH and fueling from NBI in the core, leading to a decrease of the driven ECCD and the non-inductive current fraction. ASTRA and NUBEAM modeling also reveals a strong contribution of thermal and FIs to the total plasma pressure and a reduction of the NB heating efficiency due to mainly FI CX losses. The development of plasma scenarios with either internal or external transport barriers has been pursued. ITBs were not formed in either the electron or the ion channel in the plasmas explored to date, despite a significant increase in the toroidal rotation and FI fraction with NBI, which are known to reduce turbulence. The CRONOS suite of codes has been applied in order to perform transport analyses and as a tool for the preparation of the inputs required for extended gyrokinetic simulations, which will assess whether the plasmas explored in this work are TEM turbulence dominated, therefore less prone to being stabilized. The non-inductive sustainment of plasmas with external transport barrier (H-mode) using both EC waves and NBI was successfully attempted. Nonetheless,

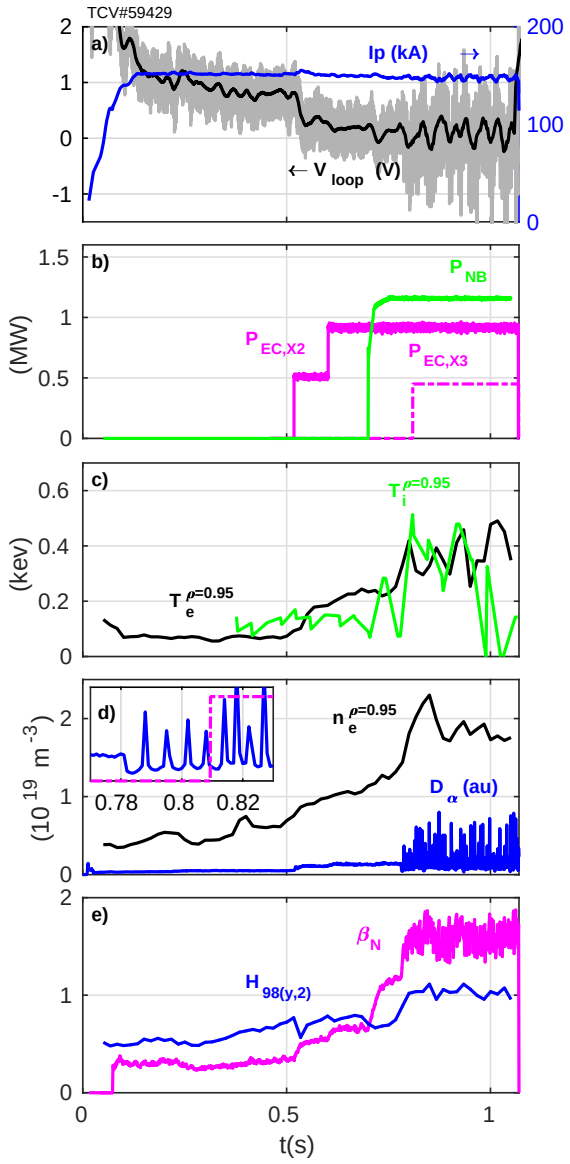

Figure 8: TCV nearly fully non-inductive H-mode plasma. Time evolution of a) the loop voltage (raw and time averaged data in gray and black on the left y-axis), the plasma current (in blue on the right y-axis); b) the ECRH power from X2 (magenta solid line) and X3 (magenta dashed line) waves and the NBI power (in green); c) the electron (in black) and the ion (in green) at the plasma pedestal; d) the electron density at the pedestal (in black) and the D_α (in blue), type-I ELMs are enlarged in the inserted plot; e) the normalized beta (in magenta) and $H_{98}(y,2)$ (in blue) .

further scenario development is needed to improve the performance and the stationarity of these plasmas. Experiments aiming at the steady-state operation of low central magnetic shear H-mode plasmas with $1 < q_0 < 2$ are going to be performed on TCV in the framework of the 2019/20 EUROfusion MST1 campaign.

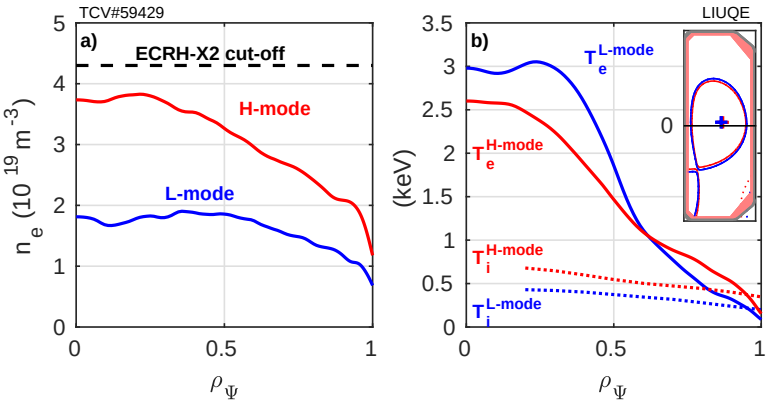

Figure 9: TCV nearly fully non-inductive H-mode plasma. Averaged L-mode (in blue) and H-mode (in red) profiles of a) the electron density from the Thomson Scattering diagnostic and b) the electron (solid line) and the ion (dotted line) from the Thomson Scattering and the CXRS diagnostic, respectively. The X2-wave cut-off density from the plasma is reported in panel a) (dashed black line). The magnetic equilibria from LIUQE with the NB injection line in the inserted plot in panel b).

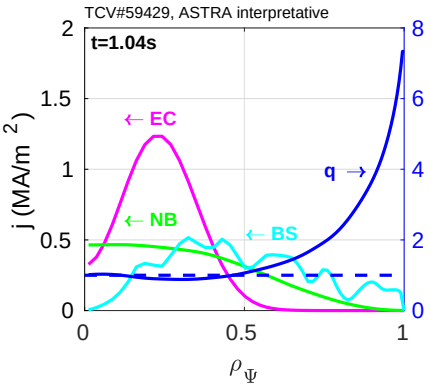

Figure 10: ASTRA interpretative modeling of a TCV nearly fully non-inductive H-mode plasma. ECRH (in magenta), NBI (in green) and bootstrap (in cyan) current density profiles (on the left y-axis) and the resulting q-profile (in blue on the right y-axis, q=1 in dashed line).

Acknowledgments

This work has been carried out within the framework of the EUROfusion Consortium and has received funding from the Euratom research and training programme 2014-2018 under grant agreement No 633053. The views and opinions expressed herein do not necessarily reflect those of the European Commission. EPFL-SPC co-authors were supported in part by the Swiss Natural Science Foundation.

References

[1] A. Karpushov *et al* 2015 Upgrade of the TCV tokamak, first phase: Neutral beam heating system *Fusion Eng. Des.* **96-97** 493-497

[2] A. Karpushov *et al* 2017 Neutral beam heating on the TCV tokamak *Fusion Eng. Des.* **123** 468-472
[3] M. Vallar *et al* 2018 Status, scientific results and technical improvements of the NBH on TCV tokamak *submitted to Fusion Eng. Des.*
[4] S. Gnesin *et al* 2012 3rd harmonic electron cyclotron resonant heating absorption enhancement by 2nd harmonic heating at the same frequency in a tokamak *Plasma Phys. Control. Fusion* **54** 035002-17
[5] S. Coda *et al* 2005 High-bootstrap, non-inductively sustained electron internal transport barrier in the Tokamak à Configuration Variable *Phys. of Plasmas* **12** 056124-1
[6] O. Sauter *et al* 2000 Steady-State Fully Non-inductive Current Driven by Electron Cyclotron Waves in Magnetically Confined Plasma *Phys. Rev. Lett.* **84** 3322-4
[7] S. Coda *et al* 2000 High-power ECH and fully non-inductive operation with ECCD in the TCV tokamak *Plasma Phys. Control. Fusion* **42** B311-B321
[8] J. K. Ehrenberg 1996 "First Wall Effects on Particle Recycling in Tokamaks", *Physical processes of the interaction of fusion plasmas with solids* **84** Academic Press, University of Michigan
[9] J. M. Moret *et al* 2015 Tokamak equilibrium reconstruction code LIUQE and its real time implementation *Fusion Eng. Des.* **91** 1-15
[10] B. LaBombard 2001 KN1D: A 1-D space, 2-D velocity, kinetic transport algorithm for atomic and molecular hydrogen in an ionizing plasma MIT PSFC Technical Report PSFC-RR-01-3 *http://www.psfc.mit.edu/∼labombard/*
[11] U. Kruezi *et al* 2012 JET divertor diagnostic upgrade for neutral gas analysis *Review of Scientific Instruments* **83**, 10D728
[12] G. Pereverzev and P. N. Yusgmanov 2002 "ASTRA - Automated System for TRansport Analysis" *IPP - Report* IPP 5/98
[13] R. J. Goldston *et al* 1981 New techniques for calculating heat and particle source rates due to neutral beam injection in axisymmetric tokamaks *J. Comp. Phys.* **43 61-78**
[14] M. Vallar *et al* 2018 Nonlinear contribution of neutral beam injection in TCV EC-heated advanced tokamak scenarios *45th European Physical Society Conference on Plasma Physics (Europhys. Conf. Abstract 42A, 2018)*
[15] B. Geiger *et al* 2017 Fast-ion transport in low density L-mode plasmas at TCV using FIDA spectroscopy and the TRANSP code *Plasma Phys. Control. Fusion* 59 115002-17
[16] L. Spitzer *et al* 1945 *Physics of Fully Ionized Gases*, Interscience Publishers Inc., New York
[17] V. F. Andreev *et al* 2016 Experimental study of density pump-out effect with on-axis electron cyclotron resonance heating at the T-10 tokamak *Plasma Phys. Control. Fusion* 58 055008-20
[18] K. Matsuda *et al* 1989 Ray Tracing Study of the Electron Cyclotron Current Drive in DIII-D Using 60 GHz *IEEE Trans. Plasma Sci.* 17 6-11
[19] C. Zucca *et al* 2009 Current density evolution in electron internal transport barrier discharges in TCV *Plasma Phys. Control. Fusion* 51 015002
[20] J. Garcia *et al* 2008 Critical Threshold Behavior for Steady-State Internal Transport Barriers in Burning Plasmas *Phys. Rev. Lett.* 100 255004
[21] S. Coda *et al* 2017 Overview of the TCV tokamak program: scientific progress and facility upgrades *Nucl. Fusion* 57 102011
[22] M. Fontana *et al* 2017 Correlation electron cyclotron emission diagnostic in TCV *Review of Scientific Instruments* 87 083506
[23] J. Garcia *et al* 2015 Key impact of finite-beta and fast ions in core and edge tokamak regions for the transition to advanced senarios *Nucl. Fusion* 55 053007-16
[24] J. F. Artaud *et al* 2010 The CRONOS suite of codes for integrated tokamak modelling *Nucl. Fusion* 50 43001- 26
[25] V. Krivenski *et al* 1985 Improving current generation in a tokamak by electron

cyclotron waves *Nucl. Fusion* **25** 127

[26] Y.R. Lin-Liu, V.S. Chan and R. Prater 2003 Electron cyclotron current drive efficiency in general tokamak geometry *Phys. Plasmas* **10** 4064

[27] M. Honda *et al* 2006 Comparison of turbulent transport models of L- and H-mode plasmas *Nucl. Fusion* **46** 580

[28] T. C. Luce Development of advanced inductive scenarios for ITER 2013 *Nucl. Fusion* **54** 013015-30